

Broadband and efficient second harmonic generation in LiNbO3-LiTaO3 composite ridge waveguides at telecom-band

Xin-Tong Zhang(张欣桐)

Citation: Chin. Phys. B, 2021, 30 (**1**): 014205. DOI: 10.1088/1674-1056/abb232
Journal homepage: http://cpb.iphy.ac.cn; http://iopscience.iop.org/cpb

What follows is a list of articles you may be interested in

Enhanced second harmonic generation in a two-dimensional optical micro-cavity

Jian-Jun Zhang(张建军), Hui-Fang Wang(王慧芳), Jun-Hua Hou(侯俊华)
Chin. Phys. B, 2018, 27 (**3**): 034207. DOI: 10.1088/1674-1056/27/3/034207

Tunable second harmonic generation from a Kerr-lens mode-locked Yb: $YCa_4O(BO_3)_3$ femtosecond laser

Zi-Ye Gao(高子叶), Jiang-Feng Zhu(朱江峰), Zheng-Mao Wu(吴正茂), Zhi-Yi Wei(魏志义), Hao-Hai Yu(于浩海), Huai-Jin Zhang(张怀金), Ji-Yang Wang(王继扬)
Chin. Phys. B, 2017, 26 (**4**): 044202. DOI: 10.1088/1674-1056/26/4/044202

Generation of femtosecond laser pulses at 396 nm in $K_3B_6O_{10}Cl$ crystal

Ning-Hua Zhang(张宁华), Hao Teng(滕浩), Hang-Dong Huang(黄杭东), Wen-Long Tian(田文龙), Jiang-Feng Zhu(朱江峰), Hong-Ping Wu(吴红萍), Shi-Lie Pan(潘世烈), Shao-Bo Fang(方少波), Zhi-Yi Wei(魏志义)
Chin. Phys. B, 2016, 25 (**12**): 124204. DOI: 10.1088/1674-1056/25/12/124204

Correction of walk-off-induced wavefront distortion for continuous-wave laser

Hongxin Zou(邹宏新), Guozhu Chen(陈国柱), Yue Wu(伍越), Yong Shen(沈咏), Qu Liu(刘曲)
Chin. Phys. B, 2016, 25 (**9**): 094211. DOI: 10.1088/1674-1056/25/9/094211

Generation of 15 W femtosecond laser pulse from a Kerr-lens mode-locked Yb: YAG thin-disk oscillator

Yingnan Peng(彭英楠), Jinwei Zhang(张金伟), Zhaohua Wang(王兆华), Jiangfeng Zhu(朱江峰), Dehua Li(李德华), Zhiyi Wei(魏志义)
Chin. Phys. B, 2016, 25 (**9**): 094207. DOI: 10.1088/1674-1056/25/9/094207

Broadband and efficient second harmonic generation in $LiNbO_3$-$LiTaO_3$ composite ridge waveguides at telecom-band

Xin-Tong Zhang(张欣桐)†

Department of Optics and Optical Engineering, University of Science and Technology of China, Hefei 230026, *China*

(Received 18 May 2020; revised manuscript received 22 June 2020; accepted manuscript online 25 August 2020)

Broadband nonlinear frequency conversions of optical waves are widely employed in multiple areas of optics and photonics. However, the broadening of conversion bandwidth is often at a cost of reduction in efficiency, which may induce a limitation on practical applications. Here we theoretically propose a novel design of $LiNbO_3$ ridge waveguides on $LiTaO_3$ substrates which can be used for efficient and broadband second harmonic generation. Through group velocity engineering of the ridge waveguides, acceptance bandwidth over 20 nm with a high conversion efficiency of $> 25\%W^{-1}\cdot cm^{-2}$ is achieved at telecom-band.

Keywords: second harmonic generation, lithium niobate ridge waveguide, dispersion manipulation

PACS: 42.65.–k, 42.65.Ky, 42.65.Wi, 42.25.–p **DOI:** 10.1088/1674-1056/abb232

1. Introduction

Second-order nonlinearity $\chi^{(2)}$ is crucial for nonlinear optical parametric processes, such as second harmonic generation (SHG), sum and difference-frequency generation (SFG/DFG). These dynamical processes are most prominent approaches to achieve modern nonlinear optical applications, including optical parametric oscillators,[1] wavelength division multiplexing,[2] super-continuum generation[3] and quantum information processing.[4] The quasi-phase-matched (QPM) wavelength conversion engineering based on periodically poled lithium niobate (PPLN) waveguides is widely employed for these applications, owing to their transparency to signal format and ultrafast interaction speed. Lithium niobate ($LiNbO_3$) crystal is a suitable $\chi^{(2)}$ material choice for wavelength conversion because of its large second order nonlinear coefficients ($d_{33} = 25$ pm/V), wide transparency range from UV to mid-IR and high refractive index. Due to these remarkable features, $LiNbO_3$ (LN) crystal becomes an efficient and prevail routine in a variety of optical and photonic applications.

Efficient wavelength conversion is essential for a range of optical applications, such as quantum storage[5] and optical frequency comb.[6] Since the nonlinear frequency conversion efficiency is related to the intensity of optical waves inside devices, $LiNbO_3$ waveguides with tight optical confinement were widely used to enhance the nonlinear interaction strength. Recently, some outstanding works based on lithium niobate thin films have been demonstrated. Peak normalized SHG efficiency of $160\%W^{-1}\cdot cm^{-2}$ has been achieved in PPLN waveguides on silicon nitride thin-film LN platforms.[7] Ultra-high wavelength conversion efficiency of $2600\%W^{-1}\cdot cm^{-2}$ has been realized by Wang using PPLNOI waveguides.[8] Luo *et al.* experimentally demonstrated a significant SHG-spectrum-tuning slope of 0.84 nm/K with a nonlinear conversion efficiency of $4.7\%W^{-1}\cdot cm^{-2}$ in a lithium niobate nano-photonic waveguide.[9] It is indicated that lithium niobate waveguides are a promising candidate for future integrated wavelength conversion systems.

Meanwhile, broad frequency conversion bandwidth is also highly desirable in many applications such as ultrafast optical signal processing, frequency tunable lasers, and optical telecommunications.[10–12] However, due to the group-velocity mismatching between interaction waves, acceptance bandwidth of highly efficient PPLN frequency conversion process is generally narrow, typically ∼50 GHz (∼0.4 nm),[13] which limits its applications in ultra-short-pulse compression,[14] frequency tunable lasers[15] and optical telecommunications.[16] Several approaches have been demonstrated to broaden the acceptance bandwidth of SHG, including aperiodic domain inverted gratings[17,18] and chirping periodically poled crystals.[19,20] However, the performance of these method is usually limited by the noticeable ripples response, fabrication difficulties, additional production costs and efficiency fluctuations.[21]

Highly efficient and simultaneously broadband second harmonic generation is of vital importance for optical applications. Ultra-broadband and efficient SHG has been realized through dispersion engineering at 2 μm wavelength,[22] whereas the specifically designed waveguide with low dispersion at 2 μm may not be applicable for dispersion properties at telecom-band. In this study, we theoretically demonstrate a broadband and efficient second harmonic generator at telecom-band, which is made of a $LiNbO_3$ ridge waveguide on a $LiTaO_3$ (LT) substrate. Through achieving simultaneously group velocity and quasi phase matching, the acceptance SHG

†Corresponding author. E-mail: zhxtong@mail.ustc.edu.cn

© 2021 Chinese Physical Society and IOP Publishing Ltd

bandwidth of >2.5 THz (~20 nm) was achieved in a 10-mm-long ridge-waveguide sample, with a conversion efficiency of >25%$W^{-1}\cdot cm^{-2}$.

2. Designed waveguide structure

Figure 1 gives a schematic view showing the overall layout of the designed waveguide structure. The $LiNbO_3$ film layer was bonded on the top of the $LiTaO_3$ substrate, both the LN film and the LT substrate were diced to form a ridge with depth of 10 μm. The $LiNbO_3$ core thickness was modulated from 2.25 μm to 3 μm for different waveguide configurations. Optical wave was restricted in the top LN layer because of the higher refractive index of LN. $LiTaO_3$ was used as the substrate material in our device because the refractive index difference between $LiNbO_3$ ($n_e = 2.13$, $n_o = 2.21$ at 1.55 μm) and $LiTaO_3$ ($n_e = 2.12$, $n_o = 2.11$ at 1.55 μm) was quite small, which effectively reduced the waveguide dispersion and contributed to a large SHG acceptance bandwidth, at telecom-band. Additionally, as the thermal expansion coefficient of $LiTaO_3$ ($\alpha = 14\times10^{-6}\ ^\circ C^{-1}$) and $LiNbO_3$ ($\alpha = 16\times10^{-6}\ ^\circ C^{-1}$) were similar, the nonlinear performance degradation and structural instability induced by thermal stress between two layers may be prevented by using the $LiTaO_3$ substrate. The solid-source MOCVD[23] and direct hetero bonding (D-HEB)[24] method were proved to be capable of fabricating a high quality single-crystal $LiNbO_3$ film on the $LiTaO_3$ substrate for waveguide applications. The fabrication of low-loss ridged $LiNbO_3$ waveguides with ultra-smooth sidewalls has been demonstrated using the optical-grade dicing method.[25–27] The above experiments proved that our device was experimentally accessible.

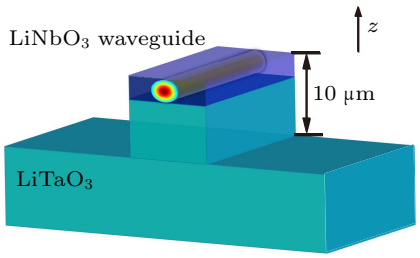


Fig. 1. Schematic diagram of the *Z*-cut $LiNbO_3$ ridge waveguide and the $LiTaO_3$ substrate.

3. SHG with birefringent phase matching

Firstly, second harmonic generation (SHG) properties, such as efficiency and acceptance bandwidth, in our device were investigated under birefringent phase matching (BPM) condition. In our simulations, the sample length was assumed to be 10 mm. The refractive index and dispersion information used in the simulation were obtained numerically from the Sellmeier equation published.[28,29] The initial pump wavelength was fixed at 1.55 μm. The temperature was tuned in a reasonable range from 20 °C to 220 °C. The designed width of the ridge waveguide was adjusted from 2 μm to 4 μm, while the $LiNbO_3$ core thickness varied from 2.25 μm to 3 μm (see Table 1). The optical guiding modes and effective indices were calculated using the FDE Eigen-mode solver simulations (Mode Solution, Lumerical Corp). Birefringent phase matching between orthogonal polarizations ($o+o\rightarrow e$, type-I modal interaction) was employed here. Although the nonlinear coefficient ($d_{31} = 4.3$ pm/V) is not comparable to that of type-0 ($e+e\rightarrow e$, $d_{33} = 25$ pm/V) interactions, the wavevector mismatch varies slowly with fundamental wavelengths under type-I interaction, which provides a broader SHG output spectrum in contrast to traditional type-0 interaction.[30,31] As shown in Fig. 2, the type-I birefringent phase matching condition was achieved in four waveguides successfully within the temperature range tunable.

No high-order modes satisfying phase matching conditions were found within the preset waveguide geometry. The fundamental transverse electric mode (TE0 for no) was phase matched with the fundamental transverse magnetic mode (TM0 for ne). The normalized conversion efficiency was calculated using the following equation:

$$\eta = \frac{8\pi^2 d_{\text{eff}}^2}{c\varepsilon_0 n_\omega^2 n_{2\omega}\lambda_\omega^2 A_{\text{eff}}}. \tag{1}$$

The effective nonlinear coefficient is $d_{\text{eff}} = d_{31} = 4.6$ pm/V, as the type-I interaction employed here. A_{eff} is the effective mode nonlinear interaction area calculated by overlap integral as follows:

$$A_{\text{eff}} = \left[\iint E_2^{\text{Nor}} E_1^{\text{Nor}} E_2^{\text{Nor}}\,\mathrm{d}x\mathrm{d}y\right]^{-2}, \tag{2}$$

where E_1^{Nor} and E_2^{Nor} are the normalized electric field profiles of the pump and the second harmonic wave. As shown in Table 1, A_{eff} is smaller in the compact waveguide, which indicates a large spatial mode overlap between the pump and SH modes. Theoretically normalized efficiency as high as 57%$W^{-1}\cdot cm^{-2}$ is achieved in waveguide 1 (WG1), with a small effective nonlinear interaction area of 3.9 μm^2.

Table 1. Details of waveguide 1 to waveguide 4.

	$LiNbO_3$ geometry sizes	A_{eff} (μm^2)	SHG efficiency (%$W^{-1}\cdot cm^{-2}$)
Waveguide 1	width = 3 μm thickness = 2 μm	3.9	57
Waveguide 2	width = 2.25 μm thickness = 3 μm	4.01	55.4
Waveguide 3	width = 2.5 μm thickness = 3 μm	4.42	50
Waveguide 4	width = 2 μm thickness = 4 μm	4.57	48.7

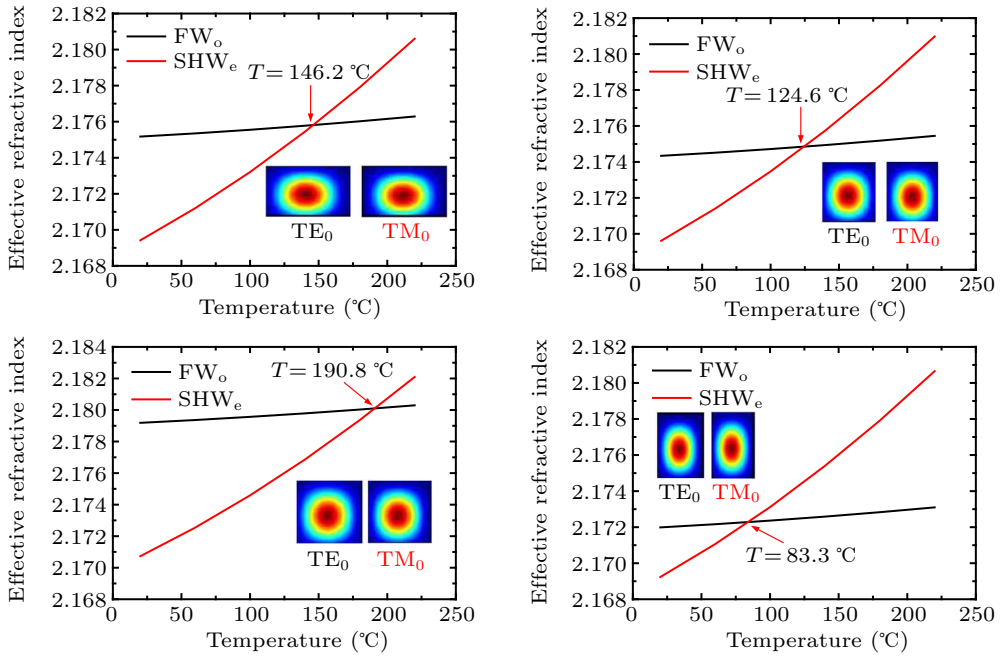


Fig. 2. Effective indices as a function of temperature under BPM conditions at the wavelength of 1550 nm in (a) WG1, (b) WG2, (c) WG3, (d) WG4 (for specific parameters see Table 1). Inset shows the modal profiles of the pump (TE_0) and SH (TM_0) waves.

WG1 (geometry size of upper LN layer: width = 3, thickness = 2) was utilized as an example in the following simulations. The SHG acceptance bandwidth of WG1 was investigated by calculating the normalized conversion efficiency. The output SHG power was proportional to phase mismatch factor given by

$$P_L \propto \mathrm{sinc}^2\left(\frac{\Delta kL}{2}\right), \tag{3}$$

where Δk was phase mismatch factor, and L was the sample length. Figure 3 illustrates the normalized SHG spectrum in WG1. A dual SHG wavelength peak was achieved. The calculated phase mismatch factor as a function of pump wavelengths was also presented. The phase match condition was satisfied ($\Delta k = 0$) under both 1520 nm and 1558 nm, at the temperature of 146.2 °C. The full width at half maximum (FWHM) of two SHG peaks were both 9 nm with the sample length of 10 mm.

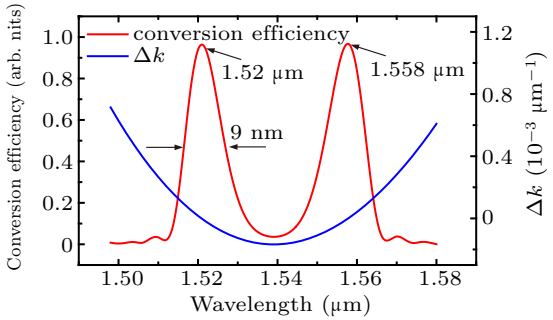


Fig. 3. SHG acceptance spectrum and mismatch factor in waveguide 1 at 146.2 °C.

The simulation results verify that the designed device shows well performance in both efficiency and spectrum responses. In WG1, the SHG efficiency is as high as 57%W^{-1}·cm^{-2}, with a broad spectrum bandwidth of 9 nm (the length of waveguide is 10 mm). The bandwidth performance is promoted compared with former high efficient SHG experiments.[7,9] It is attributed to the fact that the mismatch factor varies gently versus wavelengths in our designed device, and this character results in a wide spectrum phase matching. Additionally, in order to further broaden the SHG response bandwidth, group velocity matching is introduced in the following simulations.

4. Group velocity matching with QPM

Group-velocity mismatching results in a narrow nonlinear interaction spectrum bandwidth, because during interaction, the pump wave and SH wave walk away from each other due to the mismatch of group velocity.[32] Group-velocity matching (GVM) usually cannot be satisfied under birefringent phase matching regime, as shown in Fig. 3, the phase matching wavelengths are 1.52 μm and 1.558 μm, but the group velocity matching was satisfied under the wavelength of 1.54 μm ($\mathrm{d}\Delta k/\mathrm{d}\omega = 0$). To eliminate walk-off effect and achieve a broader SHG acceptance band, quasi-phase match (QPM) was implemented to compensate for the phase mismatch under group velocity matching condition.[13,31] The mismatch factor is defined as $\Delta k_{\mathrm{QPM}} = \Delta k - K$, where K is the QPM grating vector, given by $K = 2\pi/\Lambda$, $\Lambda = \lambda/2(n_{2\omega} - n_{\omega})$ is the period of inverted domain. The expansion term of the phase mismatch is expressed as

$$\Delta k_{\mathrm{QPM}} = \Delta k_{\mathrm{QPM}}(\omega_0) + \left(\frac{\partial \Delta k_{\mathrm{QPM}}}{\partial \omega}\right)|_{\omega_0}\delta\omega$$

$$+\frac{1}{2}\left(\frac{\partial^2 \Delta k_{\mathrm{QPM}}}{\partial \omega^2}\right)\Bigg|_{\omega_0}(\delta\omega)^2+\cdots, \tag{4}$$

the dependence of QPM mismatch factor and group velocity mismatch is given by

$$\frac{\mathrm{d}\Delta k_{\mathrm{QPM}}}{\mathrm{d}\omega}=\delta, \tag{5}$$

where $\delta = v_2^{-1} - v_1^{-1}$ is the group velocity mismatch, supposing that v_1 and v_2 are group velocities of the pump and the SH wave. It shows that the group velocity matching ($\delta = 0$) is achieved as the wave-vector mismatching takes its extremum ($\mathrm{d}\Delta k_{\mathrm{QPM}}/\mathrm{d}\omega = 0$) in the spectral region. At the group velocity matching wavelength, the mismatch factor varies negligibly versus optical frequency ($\mathrm{d}\Delta k_{\mathrm{QPM}}/\mathrm{d}\omega = 0$), QPM period (in other words, the phase mismatch factor Δk_{QPM}) can be regarded as a constant over a wide range of wavelengths, which contribute to a broadband phase matching and thus a large SHG bandwidth.[31]

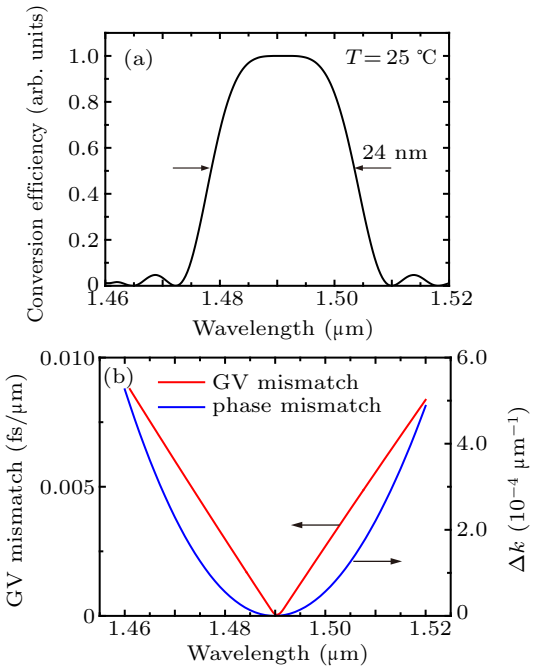


Fig. 4. (a) Acceptance bandwidth of the PPLN sample (waveguide 1) under 25 °C; (b) group-velocity mismatch and phase mismatch factor of WG1 as a function of wavelength.

The normalized QPM SHG conversion efficiency versus wavelength in WG1 with group velocity matching is illustrated in Fig. 4(a). The simulation was carried out at the room temperature (25 °C). The zero-group-velocity dispersion wavelength is 1.49 μm, where the wave-vector mismatching takes the extremum [see Fig. 4(b)]. The QPM polarization period is calculated to be 133 μm. It should be noted that the nonlinear coefficient is modulated by $\pm d_{\mathrm{eff}}$ in the QPM scheme, thus the effective nonlinear susceptibility in Eq. (1) is replaced by $d_{\mathrm{QPM}} = 2d_{31}/\pi = 3$ pm/V. The simulation results indicate that our device achieves a large SHG bandwidth of 24 nm (~3 THz) while maintains a high conversion efficiency of 25%W^{-1}·cm^{-2}, which is beneficial for wavelength conversion applications in integrated optics platforms. Meanwhile, the effects of the sample length on the SHG efficiency and the acceptance bandwidth are also investigated, as listed in Table 2.

Table 2. SHG efficiency and bandwidth related to sample length.

Length (mm)	SHG efficiency (%W^{-1})	Bandwidth (nm)
5	6.25	50
10	25	24
15	56.25	18
20	100	13

There is a trade-off between efficiency and bandwidth, because efficiency grows with the waveguide length as L^2,[33] while the bandwidth narrows because different wavelengths can accumulate different phase mismatchs (ΔkL) as L grows, according to Eq. (3). In fact, the bandwidth is decided inherently by dispersion properties of Δk, rather than the length L. Essentially, we design the waveguide to reduce the dispersion effect of Δk and to achieve a broad bandwidth, so the sample length is fixed at 10 mm in our work.

The polarization inverted voltage and electric resistance of $LiNbO_3$ decrease dramatically with magnesium oxide (MgO) doped, which is beneficial for the nonlinear characteristics and commercial applications of $LiNbO_3$. Thus, simulations were performed using the MgO-doped $LiNbO_3$ sample. The refractive index and dispersion are described by the Sellmeier equation of MgO-doped LN.[34] The calculated GVM wavelength of MgO-doped WG1 is 1.455 μm, with a conversion efficiency of 26.8%W^{-1}·cm^{-2} at room temperature. The calculated bandwidth is 23 nm with a grating period of 65 μm. The GVM wavelength is altered to communication wavelength of 1.548 μm as temperature increases to 61 °C, as illustrated by Fig. 5(a). The 3-dB acceptance bandwidth is broadened to 26 nm, at the cost of reduction in efficiency (23.8%W^{-1}·cm^{-2}). The calculated inverted domain period is 174 μm. It could be concluded that MgO-doping has little impact on SHG output features. However, it is worth noting that the crystal properties, such as non-linearity and electro-optical characteristics, will be largely promoted with MgO-doping in practical applications.

In order to investigate the SHG properties in waveguides with different geometrical parameters, the size of ridge waveguide is enlarged on the basis of WG1 (LN waveguide size: width = 3 μm, thickness = 2 μm). As depicted in Fig. 5(b) (green line), with the thickness of $LiNbO_3$ core increasing from 2 μm to 3 μm, the GVM wavelength is altered to 1.471 μm, at room temperature. The central wavelength conversion efficiency is 19%W^{-1}·cm^{-2} with acceptance bandwidth (ABW) of 25 nm. Next, the LN waveguide cross sec-

tion area is further enlarged to 4×4 μm^2, the GVM wavelength becomes 1.506 μm and the acceptance bandwidth is broadened to 27 nm while the conversion efficiency decreases to 10.6%W^{-1}·cm^{-2}. With temperature altered to 40 °C (red curve in Fig. 5(b)), the GVM wavelength of the 4×4 μm^2 cross-section waveguide is shifted to 1.545 μm. The acceptance bandwidth is as large as 28.4 nm with a grating period of 38 μm, while the conversion efficiency further decreases to 10%W^{-1}·cm^{-2}. Furthermore, as the device temperature increases, the GVM wavelength shifts with a tuning slope of 3.08 nm/°C, as shown in Fig. 5(c). Under 85 °C, the GVM wavelength is 1.69 μm, the acceptance bandwidth increases to 35 nm, due to the decrease in material dispersion at longer wavelengths.

It is concluded that as the waveguide geometry grows larger, the SHG efficiency decreases, but the bandwidth is broadened. Once the QPM and GVM are both satisfied $(\Delta k(\omega_0)=0, \Delta k'(\omega_0)=0)$, the mismatch and bandwidth are dominated by higher (second) order dispersion

$$\Delta k=\frac{1}{2}\left(\frac{\partial^2\Delta k}{\partial\omega^2}\right)\Big|_{\omega_0}(\delta\omega)^2. \tag{6}$$

Here $\Delta k''$ is induced by group velocity dispersion mismatch between fundamental wave and second harmonic wave. The second order mismatch $\Delta k''$ at GVM wavelength is calculated as listed in Table 3. $\Delta k''$ of the bulk material is also calculated for comparison.

The dispersion in waveguide devices is comprised of material dispersion and waveguide dispersion. Table 2 indicates that as the waveguide becomes more compact, the tight optical confinement introduces a stronger waveguide dispersion, which results in a narrower SHG bandwidth in our device.

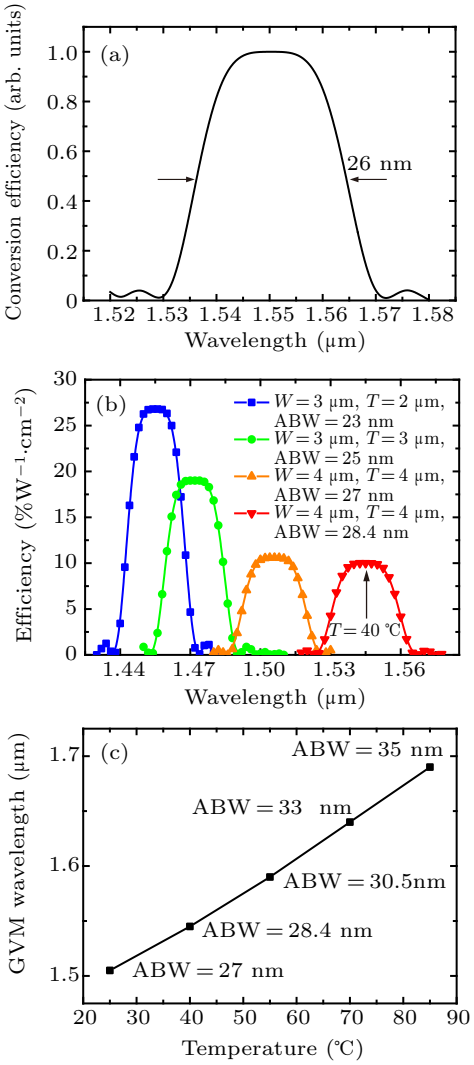


Fig. 5. (a) Normalized SHG efficiency versus wavelengths under 61 °C in MgO doped WG1; (b) GVM wavelength evolution and SHG acceptance bandwidth (ABW) of different waveguides (W: width, T: thickness); (c) GVM wavelength versus temperature in waveguide with 4×4 μm^2 cross section.

Table 3. Dispersion properties of different waveguides under GVM conditions.

Waveguide size (μm)	GVM wavelength (μm)	$\Delta k''$ (ps^2/km)	SHG bandwidth (nm)
Width = 3, thickness = 2	1.455	Total: 765.06 Bulk: 689.68 Waveguide induced: 75.37	23
Width = 3, thickness = 3	1.471	Total: 753.76 Bulk: 680.64 Waveguide induced: 73.11	25
Width = 4, thickness = 4	1.506	Total: 709.54 Bulk: 661.86 Waveguide induced: 47.67	27

Simulations were also performed with type-0 QPM configuration (e + e → e) to characterize the highest conversion efficiency by utilizing the largest non-linearity component: ($d_{\rm QPM}=2d_{33}/\pi=16$ pm/V, $d_{33}=25$ pm/V). The GVM wavelength for type-0 QPM is above 2.5 μm, far away from waveband of 1550 nm. Here, the pump wavelength is set to be 1550 nm, with the temperature of 25 °C. The simulation results are depicted in Fig. 6. Owing to the low index difference between $LiNbO_3$ ($n_e=2.13$ at 1.55 μm) waveguide and the $LiTaO_3$ ($n_e=2.12$ at 1.55 μm) substrate layer, the fundamental TM mode can only be supported in the waveguide with large $LiNbO_3$ core sizes (4×4 μm^2). The conversion efficiency as high as 303%W^{-1}·cm^{-2} is achieved theoretically, with a grating period of 15.58 μm. The SHG acceptance band-

width is only 0.41 nm, about 50 times lower than the type-I QPM interaction.

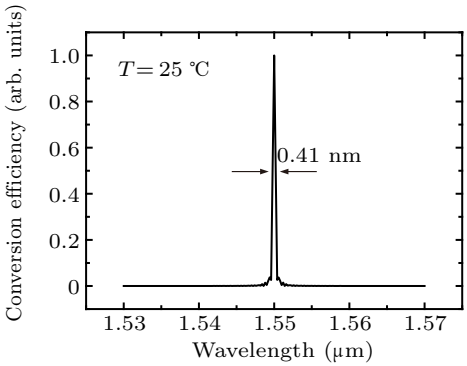


Fig. 6. SHG spectrum of type-0 interaction under wavelength of 1550 nm at 25 °C.

5. Conclusion

We have theoretically demonstrated a new type of optical waveguide composed of $LiNbO_3$ and $LiTaO_3$ materials that can be used for broadband, high-conversion-efficiency SHG at telecommunication band. By optimizing simultaneously the group-velocity and quasi-phase matching conditions in this ridge waveguide, the 3-dB acceptance bandwidth of pump wavelength can be broadened to 24 nm in a 10-mm-long sample, and the conversion efficiency can be as high as $25\%W^{-1}\cdot cm^{-2}$. We also demonstrate that several parameters of the SHG process in this waveguide, including the spectral bandwidth, conversion efficiency and central wavelength, can be tuned by adjusting the size and temperature of the waveguide. Since the $LiNbO_3$ crystal and the $LiTaO_3$ substrate have similar thermal-expansion coefficients, the waveguide structure demonstrated here has largely reduced built-in stress as the device temperature varies, allowing stable nonlinearity performance and good structure robustness.

Acknowledgment

X. T. Zhang appreciates Professor Meng Pang (Shanghai Institute of Optics and Fine Mechanics, Chinese Academy of Sciences) for his helpful advice.

References

[1] Leindecker N, Marandi A, Byer R L and Vodopyanov K L 2011 *Opt. Express* **19** 6296
[2] Gong M, Chen Y, Lu F and Chen X 2010 *Opt. Lett.* **35** 2672
[3] Phillips C R, Langrock C, Pelc J S, Fejer M M, Hartl I and Fermann M E 2011 *Opt. Express* **19** 18754
[4] Zaske S, Lenhard A, Keßler C A, Kettler J, Hepp C, Arend C, Albrecht R, Schulz W M, Jetter M, Michler P and Becher C 2012 *Phys. Rev. Lett.* **109** 147404
[5] Saglamyurek E, Jin J, Verma V B, Shaw M D, Marsili F, Nam S W, Oblak D and Tittel W 2015 *Nat. Photon.* **9** 83
[6] Mayer A S, Klenner A, Johnson A R, Luke K, Lamont M R E, Okawachi Y, Lipson M, Gaeta A L and Keller U 2015 *Opt. Express* **23** 15440
[7] Chang L, Li Y, Volet N, Wang L, Peters J and Bowers J E 2016 *Optica* **3** 531
[8] Wang C, Langrock C, Marandi A, Jankowski M, Zhang M, Desiatov B, Fejer M M and Lončar M 2018 *Optica* **5** 1438
[9] Luo R, He Y, Liang H, Li M and Lin Q 2018 *Optica* **5** 1006
[10] Chen B Q, Zhang C, Hu C Y, Liu R J and Li Z Y 2015 *Phys. Rev. Lett.* **115** 083902
[11] Zhang L, Liu Y, Jinjer H, Pu S and Yang Z 2014 *J. Opt. Soc. Am. B* **31** 1202
[12] Cardoso L, Pires H and Figueira G 2009 *Opt. Lett.* **34** 1369
[13] Ge L, Chen Y, Jiang H, Li G, Zhu B, Liu Y and Chen X 2018 *Photon. Res.* **6** 954
[14] Arbore M A, Marco O and Fejer M M 1997 *Opt. Lett.* **22** 865
[15] Breunig I, Haertle D and Buse K 2011 *Appl. Phys. B* **105** 99
[16] Oxenlowe L K, Agis F G, Ware C, Kurimura S, Mulvad H C H, Galili M, Kitamura K, Nakajima H, Ichikawa J, Erasme D, Clausen A T and Jeppesen P 2008 *Electron. Lett.* **44** 370
[17] Xianglong Z, Xianfeng C, Fei W, Yuping C, Yuxing X and Yingli C 2002 *Opt. Commun.* **204** 407
[18] Tehranchi A and Kashyap R 2008 *J. Lightw. Technol.* **26** 343
[19] Liu T, Djordjevic I, Song Z, Chen Y, Zhang R, Zhang K, Zhao W and Li B 2016 *Opt. Express* **24** 10946
[20] Lu G W, Shinada S, Furukawa H, Wada N, Miyazaki T and Ito H 2010 *Opt. Express* **18** 6064
[21] Dang W, Chen Y and Chen X 2012 *IEEE Photon. Technol. Lett.* **24** 347
[22] Jankowski M, Langrock C, Desiatov B, Marandi A, Wang C, Zhang M, Phillips C R, Lončar M and Fejer M M 2020 *Optica* **7** 40
[23] Feigelson R S 1996 *J. Cryst. Growth* **166** 1
[24] Eda K, Sugimoto M and Tomita Y 1995 *Appl. Phys. Lett.* **66** 827
[25] Takigawa R, Higurashi E, Kawanishi T and Asano T 2014 *Opt. Express* **22** 27733
[26] Courjal N, Devaux F, Gerthoffer A, Guyot C, Henrot F, Ndao A and Bernal M P 2015 *Opt. Express* **23** 13983
[27] Wang L, Haunhorst C E, Volk M F, Chen F and Kip D 2015 *Opt. Express* **23** 30188
[28] Zelmon D E, Small D L and Jundt D 1997 *J. Opt. Soc. Am. B* **14** 3319
[29] Abedin K S and Ito H 1996 *J. Appl. Phys.* **80** 6561
[30] Fejer M M, Magel G, Jundt D and Byer R 1992 *IEEE J. Quantum Electron* **28** 2631
[31] Yu N E, Ro J H, Cha M, Kurimura S and Taira T 2002 *Opt. Lett.* **27** 1046
[32] Zhong H, Zhang L, Li Y and Fan D 2015 *Sci. Rep.* **5** 10887
[33] Agrawal G P 2000 *Nonlinear Science at the Dawn of the 21st Century* (Berlin: Springer) pp. 195–211
[34] Gayer O, Sacks Z, Galun E and Arie A 2008 *Appl. Phys. B* **91** 343